PCCP

Accepted Manuscript

ROYAL SOCIETY OF CHEMISTRY

www.rsc.org/pccp

Photon-absorbing charge-bridging states in organic bulk heterojunctions consisting of diketopyrrolopyrrole derivatives and PCBM

Mikiya Fujii,[a,b,*] Woong Shin,[c] Takuma Yasuda,[c,d] and Koichi Yamashita[a,b,*]

[a]*Department of Chemical System Engineering, School of Engineering, the University of Tokyo, Tokyo, 113-8656, Japan.*

[b]*CREST, JST, 113-8656 Japan.*

[c]*INAMORI Frontier Research Center, Kyushu University, 744 Motooka, Nishi-ku, Fukuoka 819-0395, Japan.*

[d]*PRESTO, JST, 819-0395, Japan.*

*E-mail(MF): mikiya.fujii@gmail.com
*E-mail(KY): yamasita@chemsys.t.u-tokyo.ac.jp

Abstract

We have investigated the photo- and electrochemical properties of five diketopyrrolopyrrole (DPP) derivatives both experimentally and theoretically. In the experimental study, we found that a blend of DPP derivative named D2 and phenyl-C_{61}-butyric acid methyl ester (PCBM) exhibits the highest internal quantum efficiency (IQE) and power convergence efficiency (PCE) among the five derivatives investigated. In the theoretical study, we found that the open-circuit voltage can be estimated from the difference between the energy gap of frontier orbitals and voltage loss and that the latter is suppressed when IQE is large. Then, to investigate the factors that influence IQE, investigations of charge recombination, hole transfer, and charge transfer induced by photoabsorption were conducted for the complexes of each DPP derivative and PCBM. It was found that D2/PCBM exhibits the largest charge-bridging upon photoabsorption, which leads to the highest IQE and PCE among the five DPP derivatives.

Keywords

Organic solar cells, charge transfer reaction, first principles calculations, diketopyrrolopyrrole derivatives,

Introduction

The use of organic photovoltaics (OPVs) as alternative energy sources has attracted much interest in recent years. In particular, bulk heterojunction (BHJ) photovoltaic cells have many fascinating features such as high mass productivity and a lower energy requirement for production. Indeed, such devices can have very short energy payback times of as little as a few weeks.[1] After the first report of BHJ-type photovoltaic devices consisting of poly[2-methoxy-5-(3′,7′-dimethyloctyloxy)-1,4-phenylenevinylene] (MDMO-PPV) and phenyl-C_{61}-butyric acid methyl ester (PCBM) by Shaheen et al. in 2001,[2] various π-conjugated polymers have been synthesized and used to fabricate photovoltaic devices,[3–5] of which the power convergence efficiency (PCE) has recently reached more than 10%.[6]

To reveal the mechanism of generation of the photocurrent and to enhance the PCE, a range of experimental and theoretical studies have been undertaken; these investigations have examined aspects such as cool processes[7] vs hot processes[8,9] in charge separation, charge recombination,[10–13] free energy differences, [14] delocalization of the molecular orbitals,[15] molecular miscibility,[16] effects of thermal annealing,[17,18] and inverted structure cell architectures. [19] Reaction rates of the charge transfer and recombination reactions at the interface were studied in detail theoretically in the early days.[20–23] Electronic structure calculations have also been frequently adopted to reveal the charge-transfer states and effects of charge delocalization.[15,24] With regard to dynamics, structural packing between electron-donor and electron-acceptor molecules on the atomic scale are known to strongly affect the charge-transfer dynamics at the interface.[25] More recently, theoreticians have begun to reveal the energy landscape on the nanometer scale[26] and quantum dynamics calculations have also been performed in an attempt to devise ways to overcome the Coulomb interaction between electrons and holes effectively.[27–30] In general, these analyses have been performed to understand the mechanism of generation of photocurrent in the mixture of polymeric donor molecules and fullerene derivatives.

In addition to the traditional polymers, solution-processable narrow-bandgap small molecules are also attracting attention because they offer advantages such as well-defined molecular structure, intrinsic monodispersity, high purity, negligible batch-to-batch variations,

and reproducible performance. Compared with the widely studied polymer-based organic solar cells (OSCs), the development of small-molecule-based OSCs has progressed well in recent years, and PCEs of more than 9% have been reported.[31–33] Among various small molecules such as oligothiophene derivatives end-capped with electron-withdrawing units[31–40] and dithienosilole-benzothiadiazole derivatives,[41–45] diketopyrrolopyrrole (DPP) derivatives are promising candidates as donor materials for high-efficiency photovoltaics because of their high optical density and carrier transport properties. Recently, we reported DPP-based small-molecule donors that provide PCEs as high as 5.8% when combined with [6,6]-phenyl-C_{71}-butyric acid methyl ester ($PC_{71}BM$) as an electron-acceptor in OSCs.[46,47]

To develop new DPP-based small molecules that exhibit much higher PCEs and thus are promising donor materials for OPVs, we have investigated five DPP-based small-molecule donors both experimentally and theoretically. In particular, the electronic properties related to photoabsorption, recombination, and hole transfer have been investigated by using first-principles calculations.

Methods

In this study, we analyzed five donor molecules, D1–5, the chemical structures of which are shown together with PCBM as an acceptor in Fig. 1. For each of these molecules, two experiments and three sets of theoretical calculations were conducted to establish the factors that determine the efficiency of the DPP-based OPVs. In particular, theoretical analyses were performed to reveal chemical processes that could enhance or suppress the rates of photocurrent generation. The experiments conducted on the devices were (e1) UV-Vis absorption spectroscopy and (e2) current density–voltage (J–V) measurements. The theoretical calculations involved the following. (t1) Geometrical optimizations for donor molecules, pairs of donor and acceptor molecules, and dimers of donor molecules. The corresponding frontier orbitals were also analyzed. (t2) Estimation of the electronic couplings between electronic ground and charge-transfer states in the supermolecules of donor and acceptor molecules to investigate charge recombination at the interfaces. Electronic couplings between neutral and cationic donor molecules were also estimated to investigate hole transfer in the donor domain. (t3) Finally, photoexcitation inducing charge transfer simultaneously at the interfaces of donor

and acceptor molecules was analyzed.

Experimental conditions

UV-Vis absorption spectra were measured with a Shimadzu UV-2550 spectrometer. The OSC devices were fabricated according to the following procedures. ITO-coated glass substrates were cleansed sequentially by sonicating in detergent solution, deionized water, acetone, and isopropanol for 10 min each, and then subjected to UV/ozone treatment for 15 min. A thin layer (ca. 40 nm) of PEDOT:PSS (Clevios P VP Al 4083) was spin-coated onto the ITO substrate at 2000 rpm for 60 s, and then baked at 150 °C for 10 min under air. The photoactive layer was deposited by spin-casting (1000 rpm for 60 s) from a $CHCl_3$ solution containing 7–8 mg/mL of a donor and PCBM, after passing through a 0.45 μm poly(tetrafluoroethylene) filter. Finally, layers of LiF (1 nm) and Al (100 nm) were thermally evaporated on top of the active layer under high vacuum, through a shadow mask defining an active device area of 0.04 cm^2. The current density–voltage (J–V) curves of the devices were measured with a Keithley 2400 source measure unit in air under AM 1.5G solar illumination at 100 mW cm^{-2} (1 sun) with a Bunko-keiki SRO-25GD solar simulator and IPCE measurement system, calibrated with a standard Si solar cell.

Theoretical calculations

Theoretical calculations were conducted using NWChem[48] for *ab initio* calculations, e.g., Hartree–Fock (HF), density functional theory (DFT), and time-dependent density functional theory (TDDFT) and MolDS was used for the semiempirical quantum chemical method PM3.[49] Geometrical optimizations for each molecule were conducted by using DFT with basis function 6-31G* and exchange-correlation functional B3LYP.[50,51] For supermolecules such as pairs of donor and acceptor molecules and dimers of donor molecules, basis function 6-31G* and exchange-correlation functional B3LYP-D2 were adopted to include van der Waals interactions.[52] For the analysis of charge recombination and hole-transfer processes, we investigated electronic couplings between the electronic states. The electronic coupling is known as a prefactor, V_{RP}, in the Marcus theory,

$$k = \frac{2\pi}{\hbar}\sqrt{\frac{1}{4\pi\lambda k_B T}}V_{RP}^2 \exp\left[-\frac{(\Delta G_0+\lambda)^2}{4\lambda k_B T}\right], \quad (1)$$

with

$$V_{RP} = \langle \Psi_R | \, \hat{H} | \Psi_P \rangle, \quad (2)$$

where $|\Psi_R\rangle$ and $|\Psi_P\rangle$ are electronic states of the reactant and product, respectively, and $\hat{H}$ is the Hamiltonian considered. In this study, the electronic couplings for recombination and hole-transfer processes were investigated because the electronic coupling reflects the electronic transition strongly, as defined in Eq. (2). In detail, the ground and charge-transfer states were calculated with HF and constrained HF methods,[53–55] respectively, with the 6-31G* basis function, and the electronic couplings between the ground and charge-transfer states in the supermolecules of the donor and acceptor molecules were estimated. Then, the electronic couplings for hole transfers were also calculated with the constrained HF method with basis function of 6-31G*. In these calculations of electronic coupling, molecular orbitals of HF rather than DFT are used because the electronic coupling should be a transfer integral between quantum wave functions. Finally, to explore electronically excited states arising upon photoexcitation, we mainly adopted configurational interaction singles (CIS) based on the semiempirical quantum method PM3 for each DPP derivative and DPP-derivative/PCBM complex. Even today, semiempirical quantum methods are frequently used to investigate OPVs[9,56–61] because *ab initio* calculations can require huge computer resources to analyze electronic properties, such as electronic excited states of large molecules including those of OPVs. In our calculations of the electronic excited states using PM3/CIS, the number of orbitals included in the active space was set to the number of π electrons in the system. Furthermore, TDDFT with basis function 6-31G* and exchange-correlation functional CAM-B3LYP is also adopted to validate the discussion by PM3/CIS.

Results and discussion

Experimental results

Optical absorption

The experimental UV-Vis absorption spectra of the five DPP derivatives as thin films are depicted in Fig. 2. The main absorption band in the visible region is attributed to π-π* transitions in each DPP derivative. The absorption band of D1 and D2 are redshifted compared with those of D3, D4, and D5. This feature can be understood easily from the HOMO–LUMO gap and from the excited-state calculation for each DPP derivative, which will be discussed in

the theoretical section. The bimodal peak that arises in the experimental UV-Vis spectrum of D2 (582 and 637 nm) originates from packing effects of donor molecules such as J- and H-aggregates.[46] As shown in Fig. 2, D1 and D2 exhibit a relatively large photocurrent because these compounds have a broader absorption band (ca. 500 nm < λ) than the others. No specific differences in the absorption bands of D3, D4, and D5 could be observed.

Photovoltaic performance

Solution-processed BHJ solar cells were fabricated by using the five DPP derivatives as electron donors and PCBM as acceptors. Fig. 3 depicts the experimental J–V curves obtained with the BHJ solar cells based on an as-cast DPP-derivative/PCBM-blend film under AM 1.5G illumination at an intensity of 100 mW cm^{-2}. Table 1 summarizes the photovoltaic parameters of the BHJ solar cells. The internal quantum efficiencies (IQE) at 0 V presented in Table 1 were estimated from J_{SC} and from the overlap between the AM 1.5G illumination spectrum and the absorption spectrum of each DPP derivative, for which we assumed that the absorption spectra for each DPP derivative can be used to distinguish differences in these DPP derivatives. From Fig. 3 and Table 1, three prominent features are apparent: (i) the smallest V_{OC} was measured for the device with D1, (ii) the largest J_{SC} was measured for the device with D2, and thus (iii) the largest PCE (IQE) was for the device with D2. In the following theoretical analyses, we aim to explain these features in terms of electronic structures.

Theoretical calculations

Molecular orbital energies

First, the molecular structures of all DPP derivatives and PCBM were optimized. The energy levels of the frontier orbitals of the optimized structures were then calculated for each donor molecule and PCBM; these values are summarized in Table 2. The energy differences between LUMO and HOMO (ΔE_g) for each of the molecules can be used to compare the energy differences with the absorption band in Fig. 2. Thus, the smaller ΔE_g values for D1 and D2 than other DPP derivatives is consistent with the conclusion that the absorption band of D1 and D2 arise in a lower energy region than those of other DPP derivatives.

The energy differences between the LUMO of PCBM and the HOMO of each donor (ΔE_v) are also shown in Table 2. This energy difference is sometimes used as a rough estimate of the open-circuit voltage (V_{OC}). Comparing the energy differences ΔE_v to the experimental value of the open-circuit voltage, the calculated result for D1, which is minimum ΔE_v, is consistent with the lowest V_{OC} observed experimentally. Furthermore, the calculated result for D4 is also consistent with the experimental finding that the largest V_{OC} was observed for D4/PCBM. However, an exact correlation between the theoretically calculated ΔE_v and the V_{OC} measured experimentally has yet to be confirmed. This is because the open-circuit voltage is not a photovoltaic parameter that is uniquely determined by the characteristics of a single molecule; namely, the open-circuit voltage is strongly affected by various characteristics of organic semiconductors such as mobilities of charges and the extent of recombination of holes and electrons. Then, concerning the voltage loss V_{OC}^{loss}, which is defined as the difference between the theoretical ΔE_v and the experimental V_{OC} and is shown in the last row of Table 2, the order of magnitude V_{OC}^{loss} is consistent with the order of IQE. Actually, the smallest V_{OC}^{loss} value, which was obtained for D2/PCBM, is consistent with the largest IQE, which was also measured for D2/PCBM. Thus, we are now in position to discuss IQE values based on analyses of characteristics such as the mobilities of charges and the amount of recombination. Below, we focus in detail on the largest IQE of D2/PCBM. In other words, we will discuss processes that can lead to bottlenecks in the generation of photocurrent for other donors.

Electronic coupling for recombination of holes and electrons at interfaces

To investigate the magnitudes of the recombination reactions at the interfaces of each DPP derivative and PCBM, we analyzed the electronic couplings between interfacial charge-transfer and ground states. To do so, atomistic interfacial configurations needed to be optimized. Thus, we estimated the charge-transfer states for each DPP derivative/PCBM with constrained HF after the optimized structures of the supermolecules of each DPP derivative and PCBM were obtained. As an example, the optimized structure and the charge-transfer state of D2/PCBM are shown in Fig. 4 (a) and (b), respectively. In Fig. 4 (b), the difference between the electron densities of the charge-transfer and ground state is depicted; the transferred electron and the remaining hole are shown in blue and red, respectively. The electronic couplings between these

charge-transfer and ground states were then estimated for the supermolecule of each DPP derivative and PCBM; the results are summarized in Table 3. These electronic couplings reveal the extent of recombination of hole and electron at interfaces. Based on the results shown in Table 3, we can conclude that the electronic coupling of D1/PCBM is greater than those of other pairs and thus the bottleneck of the charge separation process in D1/PCBM is the recombination process.

Electronic coupling for hole transfer between DPP derivatives

In addition to the electronic couplings for recombination dynamics, we analyzed electronic couplings for hole transfer between DPP derivatives. Dimer structures for each DPP derivative were optimized before calculation of the electronic couplings for hole transfer. Two charge-localized states of the cationic dimer were then calculated by using constrained HF. In the first charge-localized state, the hole localizes on one DPP derivative. In the second charge-localized state, the hole localizes on the second DPP derivative in the dimer. As an example, the optimized structure and difference of electron densities between the two charge-localized states for D2 dimer are shown in Fig. 5 (a) and (b), respectively. In Fig. 5 (b), the densities of hole distribution before and after hole transfer are drawn in blue and red, respectively. The electronic couplings between these charge-localized states, that is, electronic couplings for hole transfer in the dimer of each DPP derivative, were then estimated; the results are summarized in Table 4. Based on these results, we can conclude that the electronic couplings for dimers of D3 and D5 are smaller than are those of the other dimers. Therefore, the bottleneck of the charge-separation process for D3/PCBM and D5/PCBM is hole transfer, because the amount of recombination increases when the holes are left as untransported carrier.

The electronic couplings of charge recombination for each DPP-derivative/PCBM complex and of hole transfer for the dimer of each of the DPP derivatives are summarized in Fig. 6. In this figure, DPP derivatives that exhibit better efficiency are shown in the upper left. We can conclude that recombination or hole transfer can be a bottleneck for the charge-separation process in D1/PCBM, D3/PCBM, and D5/PCBM. On the other hand, these elementary processes cannot be a bottleneck for D2/PCBM and D4/PCBM. Indeed, experimental results show that D2/PCBM and D4/PCBM exhibit higher IQE (see Table 1). In

the following, we discuss the differences between D2 and D4 and clarify why a superior quantum efficiency is observed for D2/PCBM.

Direct charge transfer induced by photoexcitation

Recently, Yu et al. demonstrated that the absolute value of the change in dipole moment before and after photoexcitation of the donor correlates strongly with the magnitude of the short-circuit current density.[57] Namely, donors that exhibit a large change in dipole moment upon photoexcitation can create pairs of holes and electrons in the donor molecule that can be separated more easily. For analysis of the change of dipole, electronic excited states are needed. In this study, the semiempirical PM3 method was mainly adopted to calculate the excited states. The oscillator strengths of the electronic excited states were then estimated with CIS based on PM3 for each DPP derivative (Fig. 7). We can conclude from this figure that the photoabsorbing states of D3 (480 nm), D4 (491 nm), and D5 (483 nm) are slightly blueshifted compared with those of D1 (567 nm) and D2 (534 nm), which is quantitatively consistent with the experimental results shown in Fig. 2. The bimodal peak that only arises in the experimental UV-Vis spectrum of D2 (582 and 637 nm in the spectrum plotted in red in Fig. 2) is due to the packing of donor molecules such as J- and H-aggregates.[46] Detailed analysis of bimodal spectra of this type is beyond the scope of this study; here, we concentrate on a theoretical analysis of each isolated donor molecule. The semiempirical PM3/CIS method delivers sufficient precision for the calculations of electronic excited states necessary for the present discussion.

In Table 5, the change of the dipole moment between the ground state and excited state that exhibits the highest oscillator strength is summarized as $\Delta\mu_D$ for all DPP derivatives. However, no correlation with IQE was found for the DPP derivatives because they do not exhibit intramolecular charge transfer. The same analysis of change in the dipole moment was then applied to each DPP-derivative/PCBM complex. The change in dipole moment that is induced upon photoexcitation of each DPP-derivative/PCBM complex ($\Delta\mu_{D/A}$) is also summarized in Table 5. As can be seen in this table, the changes of the dipole moment in D2/PCBM and D4/PCBM are greater than those of other DPP-derivative/PCBM complexes. In particular, the change of the dipole moment in D2/PCBM is greater than that of D4/PCBM. These changes in the dipole $\Delta\mu_{D/A}$ arise from changes in charge distribution on the DPP-

derivative/PCBM complexes. Especially, the trend in the change of the dipole moment $\Delta\mu_{D/A}$ that is induced by photoexcitation of DPP-derivative/PCBM complexes is consistent with the trend of the IQE values observed experimentally, as shown in Table 1.

To reveal the physical mechanism of the correlation between the large change of dipole moment and IQE, we recorded the UV-Vis spectra of complexes of the DPP derivative and PCBM. Fig. 8 shows the calculated UV-Vis spectra for D2 alone and for the D2/PCBM complex, which are shown in red and blue, respectively. The excited state that has the highest oscillator strength for the donor excitation (534 nm for D2) is slightly redshifted (550 nm for D2/PCBM) due to the interaction with PCBM. Furthermore, the oscillator strength is also reduced due to the interaction with PCBM. The principal molecular orbitals that contribute to the UV-Vis spectra are shown in Fig. 9. Donor excitation at 534 nm arises from HOMO–LUMO transition of the D2 molecule, the MOs of which are shown in Fig. 9 (a) and (b), respectively. On the other hand, the states that hold the largest oscillator strength in the D2/PCBM complex originate mainly from a single electron excitation from HOMO to LUMO+5 of D2/PCBM; these are shown in Fig. 9 (c) and (d), respectively. The donor part in Fig. 9 (c) and (d) originates from the HOMO and LUMO of the donor, respectively. Therefore, the ability to absorb a photon is retained in the D2/PCBM complex. Notably, the LUMO+5 molecular orbital of the D2/PCBM complex is delocalized on to the acceptor part. Orbitals that are delocalized over both the donor and the acceptor are called *charge-bridging orbitals*.[24] Therefore, photoexcitation of D2/PCBM at 550 nm is understood as photoexcitation from the HOMO of D2 to the charge-bridging orbital of the D2/PCBM complex.

In Table S1-1 of supplementary information, we summarized three main configurations of the photo-absorbing states of complexes of each DPP-derivative and PCBM, which were obtained by PM3/CIS calculations. Besides, main contributing molecular orbitals are also shown in Figure S1-1. One can confirm from Figure S1-1 and Table S1-1 that the photo-absorbing state (1^{st} excited state) of D2/PCBM holds the most strongest charge-bridging nature among the five complexes. Especially, at the molecular interface of the D2 and PCBM, electron population is denser than other complexes. This is the reason why photoexcitation of D2/PCBM induces the largest changes of dipole moment. Therefore, we consider that these partial charge-bridging orbitals ~~transfer states~~ which can absorb a photon are critical for enhancing the charge separation in OSCs because

they create pairs of electrons and holes which can separate easily. We hereafter term this states holding the charge-bridging orbital as, which is induced by photon absorption directly, as a photon-absorbing charge-bridging (PACB) state.

To validate this PACB~~T~~ state in D2/PCBM, we conducted TDDFT calculations with basis function 6-31G* and exchange-correlation functional CAM-B3LYP also. The calculated UV-Vis spectra of complexes of the DPP derivative and PCBM are shown in Fig. 10 (a). By comparison of this calculated UV-Vis spectra with those calculated by PM3/CIS, we can confirm that PM3/CIS spectra delivering sufficient precision for the present discussion. Besides, we also estimated numerical correction which was introduced by adopting larger basis function, 6-31+G*, through rough estimation of energies of the charge transfer states as differences of the ionization energy of P3HT and the electron affinity of PCBM. Then, we conclude that the estimated correction to the UV-Vis spectra by expanding the electronic Hilbert space is 0.19 eV even for the charge transfer states. The detail in estimating of the numerical correction is explained in supplementary information (Sec. S2). In Fig. 10 (b) and (c), HOMO and LUMO+2 of PCBM/D2 complex, which are calculated with TDDFT/CAM-B3LYP/6-31G*, are shown, respectively. Note that the LUMO+2 is the *charge-bridging orbital*. The electronic configuration in which an electron is excited from HOMO to LUMO+2 is the main configuration of the prominent photo-absorbing state of PCBM/D2. Namely, considering that LUMO+2 is the charge-bridging orbital, we can validate the charge-bridging nature of photo-absorbing state of PCBM/D2.

In Table S3-1 of supplementary information, we also summarized three main configurations of the photo-absorbing states of complexes of each DPP-derivative and PCBM, which were obtained by TDDFT/Cam-B3LYP/6-31G* calculations. Besides, the main contributing molecular (Kohn-Sham) orbitals are shown in Figure S3-1. One can confirm from Figure S3-1 and Table S3-1 that the photo-absorbing state (5^{th} excited state) of D2/PCBM exhibiting the most strongest charge-bridging nature among the five complexes. Especially, at the molecular interface of the D2 and PCBM, electron population is denser than other complexes as well as results obtained by PM3/CIS. Namely, these results obtained with TDDFT/CAM-B3LYP/6-31G* are qualitatively consistent to the photon-absorbing charge-bridging orbitals, which was discussed by using with PM3/CIS.

Finally, we conclude that the existence of PACB states, which is a physical origin of large

change of dipole moment, is crucial for enhancing IQE because the bounded electron and hole in PACB states should separate to free carriers more easily than those in the usual donor-excited states.

Summary and conclusions

We have investigated five DPP derivatives both experimentally and theoretically. In the experimental part, we found that the blend of DPP derivative D2 and PCBM exhibits the highest IQE and PCE among the five DPP derivatives. In the theoretical part, we found that the open-circuit voltage V_{OC} can be estimated from the difference between the energy gap of the frontier orbitals E_v and the voltage loss V_{OC}^{loss} and that the latter is suppressed when IQE is large. Given that the short-circuit current density is clearly enhanced when IQE is large, we proceeded to analyze the IQE theoretically by investigating charge recombination, hole transfer, and charge transfer induced by photoabsorption to reveal bottlenecks or factors that enhance photocurrent generation.

The computational results revealed the following features of each DPP derivative. In D1/PCBM, charge recombination at the interface suppresses IQE because of large electronic coupling between the ground and interfacial charge-transfer states. In D3/PCBM and D5/PCBM, the low hole mobility that increases the amount of recombination suppresses IQE. In contrast to these derivatives, charge recombination and hole transfer could not become the bottleneck of the charge-separation processes for D2/PCBM and D4/PCBM. Both of the latter two complexes also exhibit larger direct charge transfer induced by photon absorption. In particular, D2/PCBM exhibits the largest PACB states, from which charge separation to free carriers should occur easily. Even if the main absorber of photons is the bulk donor, the charge-bridging states can enhance the charge-generation as additive photon-absorbers at the interface or intermediate states of the charge separation started from donor-excitons. PACB, therefore, leads to the highest IQE and PCE for the D2/PCBM complex among the five DPP derivatives.

Although it may be challenging to observe the photon-absorbing charge-bridging orbitals directly as experimental observables, some theoretical studies have investigated these concepts for poly-3-hexylthiophene (P3HT)/PCBM.[24,62,63] In addition to these past studies, the present study also stresses the important role of charge-bridging orbitals. It is expected that

these concepts should help clarify the process of charge separation in OSCs.

Acknowledgement

This work was supported by JSPS KAKENHI Grant No. 24750012, CREST JST, and PRESTO JST. Theoretical calculations in this study were performed using facilities at Supercomputer Center in Institute for Solid State Physics (ISSP) of University of Tokyo and at Research Center for Computational Science in Institute for Molecular Science (IMS) in Okazaki, Japan.

References

(1) R. Gaudiana and C. Brabec, Organic materials: Fantastic plastic. *Nat. Photo.* **2008**, *2*, 287–289.

(2) S. E. Shaheen, C. J. Brabec, N. S. Sariciftci, F. Padinger, T. Fromherz, and J. C. Hummelen, 2.5% efficient organic plastic solar cells. *App. Phys. Lett.* **2001**, *78*, 841–843.

(3) S. Günes, H. Neugebauer, and N. S. Sariciftci, Efficiency of bulk-heterojunction organic solar cells. *Chem. Rev.* **2007**, *107*, 1324–1338.

(4) A. W. Hains, Z. Liang, M. A. Woodhouse, and B. A. Gregg, Molecular Semiconductors in Organic Photovoltaic Cells. *Chem. Rev.* **2010**, *110*, 6689–6735.

(5) T. M. Clarke and J. R. Durrant, Charge Photogeneration in Organic Solar Cells. *Chem. Rev.* **2010**, *110*, 6736–6767.

(6) M. A. Green, K. Emery, Y. Hishikawa, W. Warta and E. D. Dunlop, Solar cell efficiency tables (Version 45), Prog. Photovolt: Res. Appl. **2015**, 23,1–9

(7) K. Vandewal, S. Albrecht, E. T. Hoke, K. R. Graham, J. Widmer, J. D. Douglas, M. Schubert, W. R. Mateker, J. T. Bloking, G. F. Burkhard, A. Sellinger, J. M. J. Fréchet, A. Amassian, M. K. Riede, M. D. McGehee, D. Neher, and A. Salleo, Efficientt charge generation by relaxed charge-transfer states at organic interfaces. *Nat. Mat.* **2014**, *13*, 63–68.

(8) A. E. Jailaubekov, A. P. Willard, J. R. Tritsch, W.-L. Chan, N. Sai, R. Gearba, L. G. Kaake, K. J. Williams, K. Leung, P. J. Rossky, and X-Y. Zhu, Hot charge-transfer excitons set the time limit for charge separation at donor/acceptor interfaces in organic photovoltaics. *Nat. Mat.* **2013**, *12*, 66–73.

(9) G. Grancini, M. Maiuri, D. Fazzi, A. Petrozza, H.-J. Egelhaaf, D. Brida, G. Cerullo, and G. Lanzani, Hot exciton dissociation in polymer solar cells. *Nat. Mat.* **2013**, *12*, 29–33.

(10) J. Guo, H. Ohkita, H. Benten, and S. Ito, Charge Generation and Recombination Dynamics in Poly(3-hexylthiophene)/Fullerene Blend Films with Different Regioregularities and Morphologies. *J. Am. Chem. Soc.* **2010**, *132*, 6154–6164.

(11) R. Mauer, I. A. Howard, and F. Laquai, Effect of Nongeminate Recombination on Fill Factor in Polythiophene/Methanofullerene Organic Solar Cells. *J. Phys. Chem. Lett.* **2010**, *1*, 3500–3505.

(12) F. Etzold, I. A. Howard, R. Mauer, M. Meister, T.-D. Kim, K.-S. Lee, N. S. Baek, and F. Laquai, Ultrafast Exciton Dissociation Followed by Nongeminate Charge Recombination in PCDTBT:PCBM Photovoltaic Blends. *J. Am. Chem. Soc.* **2011**, *133*, 9469– 9479.

(13) C. M. Proctora, M. Kuika, and T.-Q. Nguyena, Charge carrier recombination in organic solar cells. *Prog. Polym. Sci.* **2013**, *38*, 1941–1960.

(14) H. Ohkita, S. Cook,Y. Astuti, W. Duffy, S. Tierney, W. Zhang, M. Heeney, I. McCulloch, J. Nelson, D. D. C. Bradley, and J. R. Durrant. Charge Carrier Formation in Polythiophene/Fullerene Blend Films Studied by Transient Absorption Spectroscopy. *J. Am. Chem. Soc.* **2008**, *130*, 3030–3042.

(15) A. A. Bakulin, A. Rao, V. G. Pavelyev, P. H. M. van Loosdrecht, M. S. Pshenichnikov, D. Niedzialek, J. Cornil, D. Beljonne, and R. H. Friend, The Role of Driving Energy and Delocalized States for Charge Separation in Organic Semiconductors. *Science* **2012**, *335*, 1340–1344.

(16) B. A. Collins, E. Gann, L. Guignard, X. He, C. R. McNeill, and H. Ade, Molecular Miscibility of Polymer-Fullerene Blends. *J. Phys. Chem. Lett.* **2010**, *1*, 3160–3166.

(17) N. D. Treat, M. A. Brady, G. Smith, M. F. Toney, E. J. Kramer, C. J. Hawker, and M. L. Chabinyc, Interdiffusion of PCBM and P3HT Reveals Miscibility in a Photo-voltaically Active Blend. *Adv. Energy Mater.* **2011**, *1*, 82–89.

(18) D. Mori, H. Benten, H. Ohkita, and S. Ito, Morphology-Limited Free Carrier Generation in Donor/ Acceptor Polymer Blend Solar Cells Composed of Poly(3-hexylthiophene) and Fluorene-Based Copolymer. *Adv. Energy Mater.* **2011**, *5*, 1500304.

(19) V. Vohra, K. Kawashima, T. Kakara, T. Koganezawa, I. Osaka, K. Takimiya, and H. Murata, Efficient inverted polymer solar cells employing favourable molecular orientation, Nature Photo. **2015**, 9, 403–408

(20) P. van Hal, S. C. J. Meskers, and R. A. J. Janssen, Photoinduced energy and electron transfer in oligo(p-phenylene vinylene)-fullerene dyads. *J. Appl. Phys. A* **2004**, *79*, 41–46.

(21) T. Kawatsu, V. Coropceanu, A. Ye, and J.-L. Brédas, Quantum Chemical Approach to Electronic Coupling: Application to Charge Separation and Charge Recombination Pathways in a Model Molecular Donor-Acceptor System for Organic Solar Cells. *J. Phys. Chem. C* **2008**, *112*, 3429–3433.

(22) Y. Yi, V. Coropceanu, and J.-L. Brédas, Exciton-Dissociation and Charge-Recombination Processes in Pentacene/C60 Solar Cells: Theoretical Insight into the Impact of Interface Geometry. *J. Am. Chem. Soc.* **2009**, *131*, 15777–15783.

(23) T. Liu and A. Troisi, Absolute Rate of Charge Separation and Recombination in a Molecular Model of the P3HT/PCBM Interface. *J. Phys. Chem. C* **2011**, *115*, 2406–2415.

(24) T. Liu, D. L. Cheunga, and A. Troisi, Structural variability and dynamics of the P3HT/PCBM interface and its effects on the electronic structure and the charge-transfer rates in solar cells. *Phys. Chem. Chem. Phys.* **2011**, *13*, 21461–21470.

(25) M. Fujii and K. Yamashita, Packing effects in organic donor – acceptor molecular heterojunctions. *Chem. Phys. Lett.* **2012**, *514*, 146–150.

(26) G. D'Avino, S. Mothy, L. Muccioli, C. Zannoni, L. Wang, J. Cornil, D. Beljonne, and F. Castet, Energetics of Electron – Hole Separation at P3HT/PCBM Heterojunctions. *J. Phys. Chem. C* **2013**, *117*, 12981–12990.

(27) H. Tamuraa, I. Burghardt, and M. Tsukada, Exciton Dissociation at Thiophene/Fullerene Interfaces: The Electronic Structures and Quantum Dynamic. *J. Phys. Chem. C* **2011**, *115*, 10205–10210.

(28) H. Tamura, R. Marinazzo, M. Ruckenbauer, and I. Burghardt, Quantum dynamics of ultrafast charge transfer at a polymer-fullerene interface. *J. Chem. Phys.* **2012**, *137*, 22A540.

(29) H. Tamura and I. Burghardt, Ultrafast Charge Separation in Organic Photovoltaics Enhanced by Charge Delocalization and Vibronically Hot Exciton Dissociation. *J. Am. Chem. Soc.* **2013**, *135*, 16364–16367.

(30) E. Bittner and C. Silva, Noise-induced quantum coherence drives photo-carrier generation dynamics at polymeric semiconductor heterojunctions. *Nat. Comm.* **2013**, *5*, 3119.

(31) B. Kan, M. Li, Q. Zhang, F. Liu, X. Wan, Y. Wang, W. Ni, G. Long, X. Yang, H. Feng, Y. Zuo, M. Zhang, F. Huang, Y. Cao, T. P. Russell and Y. Chen, A Series of Simple Oligomer-like Small Molecules Based on Oligothiophenes for Solution-Processed Solar Cells with High Efficiency. *J. Am. Chem. Soc.* **2015**, *137*, 3886–3893.

(32) B. Kan, Q. Zhang, M. Li, X. Wan, W. Ni, G. Long, Y. Wang, X. Yang, H. Feng and Y. Chen, Solution-Processed Organic Solar Cells Based on Dialkylthiol-Substituted Benzothiophene Unit with Efficiency near 10%. *J. Am. Chem. Soc.* **2014**, *136*, 15529–15532.

(33) K. Sun, Z. Xiao, S. Lu, W. Zajaczkowski, W. Pisula, E. Hanssen, J. M. White, R. M. Williamson, J. Subbiah, J. Ouyang, A. B. Holmes, W. W. H. Wong, and D. J. Jones, A molecular nematic liquid crystalline material for high-performance organic photovoltaics. *Nat. Commun.* **2015**, 7013.

(34) Y. Liu, C.-C. Chen, Z. Hong, J. Gao, Y. M. Yang, H. Zhou, L. Dou, G. Li, and Y.

Yang, Solution-processed small-molecule solar cells: breaking the 10% power conversion efficiency. *Sci. Rep.* **2013**, *3*, 3356.

(35) J. Zhou, X. Wan, Y. Liu, G. Long, F. Wang, Z. Li, Y. Zuo, C. Li, and Y. Chen, A Planar Small Molecule with Dithienosilole Core for High Efficiency Solution-Processed Organic Photovoltaic Cells. *Chem. Mater.* **2011**, *23*, 4666–4668.

(36) J. Zhou, X. Wan, Y. Liu, Y. Zuo, Z. Li, G. He, G. Long, W. Ni, C. Li, X. Su, and Y. Chen, Small Molecules Based on Benzo[1,2-b:4,5-b′]dithiophene Unit for High-Performance Solution-Processed Organic Solar Cells. *J. Am. Chem. Soc.* **2012**, *134*, 16345–16351.

(37) J. Zhou, Y. Zuo, X. Wan, G. Long, Q. Zhang, W. Ni, Y. Liu, Z. Li, G. He, C. Li, B. Kan, M. Li, and Y. Chen, Solution-Processed and High-Performance Organic Solar Cells Using Small Molecules with a Benzodithiophene Unit. *J. Am. Chem. Soc.* **2013**, *135*, 8484–8487.

(38) Y. Liu, X. Wan, F. Wang, J. Zhou, G. Long, J. Tian, J. You, Y. Yang, and Y. Chen, Spin-Coated Small Molecules for High Performance Solar Cells. *Adv. Energy Mater.* **2011**, *1*, 771–775.

(39) Z. Li, G. He, X. Wan, Y. Liu, J. Zhou, G. Long, Y. Zuo, M. Zhang, and Y. Chen, Solution Processable Rhodanine-Based Small Molecule Organic Photovoltaic Cells with a Power Conversion Efficiency of 6.1%. *Adv. Energy Mater.* **2012**, *2*, 74–77.

(40) R. Fitzner, E. Mena-Osteritz, A. Mishra, G. Schulz, E. Reinold, M. Weil, C. Körner, H. Ziehlke, C. Elschner, K. Leo, M. Riede, M. Pfeiffer, C. Uhrich, and P. Bäuerle, Correlation of π-Conjugated Oligomer Structure with Film Morphology and Organic Solar Cell Performance. *J. Am. Chem. Soc.* **2012**, *134*, 11064–11067.

(41) Y. Sun, G. C. Welch, W. L. Leong, C. J. Takacs, G. C. Bazan, and A. J. Heeger, Solution-processed small-molecule solar cells with 6.7% efficiency. *Nat. Mat.* **2012**, *11*, 44–48.

(42) V. Gupta, A. K. K. Kyaw, D. H. Wang, S. Chand, G. C. Bazan, and A. J. Heeger, Barium: an efficient cathode layer for bulk-heterojunction solar cells. *Sci. Rep.* **2013**, *3*, 1965.

(43) A. K. K. Kyaw, D. H. Wang, V. Gupta, J. Zhang, S. Chand, G. C. Bazan, and A. J. Heeger, Efficient Solution-Processed Small-Molecule Solar Cells with Inverted Structure. *Adv. Mat.* **2013**, *25*, 2397–2402.

(44) X. Liu, Y. Sun, L. A. Perez, W. Wen, M. F. Toney, A. J. Heeger, and G. C. Bazan, Narrow-Band-Gap Conjugated Chromophores with Extended Molecular Lengths. *J. Am. Chem. Soc.* **2012**, *134*, 20609–20612.

(45) C. J. Takacs, Y. Sun, G. C. Welch, L. A. Perez, X. Liu, W. Wen, G. C. Bazan, and A. J. Heeger, Solar Cell Efficiency, Self-Assembly, and Dipole–Dipole Interactions of Isomorphic Narrow-Band-Gap Molecules. *J. Am. Chem. Soc.* **2012**, *134*, 16597–16606.

(46) W. Shin, T. Yasuda, G. Watanabe, Y. S. Yang, and C. Adachi, Self-Organizing Mesomorphic Diketopyrrolopyrrole Derivatives for Efficient Solution-Processed Organic Solar Cells. *Chem. Mater.* **2013**, *25*, 2549–2556.

(47) W. Shin, T. Yasuda, Y. Hidaka, G. Watanabe, R. Arai, K. Nasu, T. Yamaguchi, W. Murakami, K. Makita, and C. Adachi, π-Extended Narrow-Bandgap Diketopyrrolopyrrole-Based Oligomers for Solution-Processed Inverted Organic Solar Cells. *Adv. Energy Mater.* **2014**, *4*, 1400879.

(48) M. Valiev, E. Bylaska, N. Govind, K. Kowalski, T. P. Straatsma, H. J. J. Van Dam, D. Wang, J. Nieplocha, E. Apra, T. L. Windus, and W.A. de Jong, NWChem: A comprehensive and scalable open-source solution for large scale molecular simulations. *Comp. Phys. Comm.* **2010**, *181*, 1477–1489.

(49) J. J. P. Stewart, Optimization of parameters for semiempirical methods I. Method. *J. Comp. Chem.* **1989**, *10*, 209–220.

(50) A. D. Becke, Density-functional exchange-energy approximation with correct asymptotic behavior. *Phys. Rev. A* **1988**, *38*, 3098–3100.

(51) C. Lee, W. Yang, and R. G. Parr, Development of the Colle-Salvetti correlation-energy formula into a functional of the electron density. *Phys. Rev. B* **1988**, *37*, 785–789.

(52) S. Grimme, Semiempirical GGA-type density functional constructed with a long-range dispersion correction. *J. Comp. Chem.* **2006**, *27*, 1787–1799.

(53) Q. Wu and T. V. Voorhis, Direct optimization method to study constrained systems within density-functional theory. *Phys. Rev. A* **2005**, *72*, 024502.

(54) Q. Wu and T. V. Voorhis, Constrained Density Functional Theory and Its Application in Long-Range Electron Transfer. *J. Chem. Theory Comput.* **2006**, *2*, 765–774.

(55) Y. Yamagata, Y. Imamuraa and H. Nakai, Constrained self-consistent field method revisited toward theoretical designs of functional materials under external field *Chem. Phys. Lett.* **2012**, *530*, 132–136.

(56) X. Zhang, T. T. Steckler, R. R. Dasari, S. Ohira, W. J. Potscavage, Jr., S. P. Tiwari, S. Coppé, S. Ellinger, S. Barlow, J.-L. Brédas, B. Kippelen, J. R. Reynolds, and S. R. Marder, Dithienopyrrole-based donor-acceptor copolymers: low band-gap materials for charge transport, photovoltaics and electrochromism. *J. Mater. Chem.* **2010**, *20*, 123–134.

(57) B. Carsten, J. M. Szarko, H. J. Son, W. Wang, L. Lu, F. He, B. S. Rolczynski, S. Lou, L. X. Chen, and L. Yu, Examining the Effect of the Dipole Moment on Charge Separation in Donor – Acceptor Polymers for Organic Photovoltaic Applications. *J. Am. Chem. Soc.* **2011**, *133*, 20468–20475.

(58) I. Y. Kanal, S. G. Owens, J. S. Bechtel, and G. R. Hutchison, Efficient Computational Screening of Organic Polymer Photovoltaics. *J. Phys. Chem. Lett.* **2013**, *4*, 1613–1623.

(59) F. Zamora, R. A. Vázquez, J. Coreño, I. Moggio, E. Arias, R. Flores, and A de León,

Optical properties of a new p-phenylenevinylene oligomer containing quinolines and ferrocene for organic solar cells. *Materials Science and Engineering* **2013**, *45*, 6049–6055.

(60) T. Qin, W. Zajaczkowski, W. Pisula, M. Baumgarten, M. Chen, M. Gao, G. Wilson, C. D. Easton, K. Müllen, and S. E. Watkins, Tailored Donor − Acceptor Polymers with an A − D1 − A − D2 Structure: Controlling Intermolecular Interactions to Enable Enhanced Polymer Photovoltaic Devices. *J. Am. Chem. Soc.* **2014**, *136*, 6049–6055.

(61) F. Wong, G. Perez, M. Bonilla, J. A. Colon-Santana, X. Zhang, P. Sharma, A. Gruverman, P. A. Dowbenc, and L. G. Rosa, Changing molecular band offsets in polymer blends of (P3HT/P(VDF-TrFE)) poly(3-hexylthiophene) and poly(vinylidene fluoride with trifluoroethylene) due to ferroelectric poling. *RSC Adv.* **2014**, *4*, 3023–3027.

(62) Y. Kanai and J. C. Grossman, Insights on Interfacial Charge Transfer Across P3HT/Fullerene Photovoltaic Heterojunction from Ab Initio Calculations. *Nano Lett.* **2007**, *7*, 1967–1972.

(63) Z. Li, X. Zhang, and G. Lu, Electron structure and dynamics at poly(3-hexylthiophene)/fullerene photovoltaic heterojunctions. *App. Phys. Lett.* **2011**, *98*, 083303.

Table 1: Photovoltaic parameters for the solution-processed BHJ solar cells.

	D/A ratio wt/wt	h/nm	J_{SC}/mAcm^{-2}	V_{OC}/V	FF/%	PCE/%	IQE/%
D1	1:1	95	–2.13	0.43	52.3	0.48	16.0
D2	1:1	107	–5.74	0.94	38.7	2.09	50.2
D3	1:1	96	–0.88	0.85	25.6	0.19	12.2
D4	1:1	91	–1.52	1.05	27.9	0.44	22.1
D5	1:1	123	–0.67	0.75	26.7	0.13	8.87

Table 2: E_{HOMO}, E_{LUMO}: Energy levels of the frontier orbitals of the optimized structures for the donors and PCBM. ΔE_g: Energy differences between LUMO and HOMO for all donors. ΔE_v: Energy differences between LUMO of PCBM and HOMO of each donor. V_{OC}^{loss}: Energy difference between the theoretical ΔE_v and the experimental V_{OC}. All values are shown in electron volts (eV).

	D1	D2	D3	D4	D5	PCBM
E_{HOMO}	–4.63	–4.72	–4.90	–4.89	–5.02	–5.55
E_{LUMO}	–2.63	–2.50	–2.43	–2.50	–2.56	–2.98
ΔE_g	2.00	2.22	2.47	2.34	2.46	2.56
ΔE_v	1.65	1.74	1.92	1.91	2.04	–
V_{OC}^{loss}	1.22	0.80	1.07	0.86	1.29	–

Table 3: Electronic coupling V_{RP} for charge recombination.

	D1	D2	D3	D4	D5
V_{RP} /eV	0.0637	0.0466	0.0500	0.0385	0.00682

Table 4: Electronic coupling V_{RP} for hole transfer.

	D1	D2	D3	D4	D5
V_{RP} /eV	0.196	0.112	0.030	0.065	0.0312

Table 5: Change of the dipole moment induced upon photoexcitation of donor molecules ($\Delta\mu_D$) and DPP-derivative/PCBM complexes ($\Delta\mu_{D/A}$).

	D1	D2	D3	D4	D5
$\Delta\mu_D$/D	4.75×10^{-2}	8.94×10^{-2}	4.06×10^{-1}	4.18×10^{-1}	3.41×10^{-1}
$\Delta\mu_{D/A}$/D	3.73	4.05	2.88	3.89	2.18

Graphical abstract

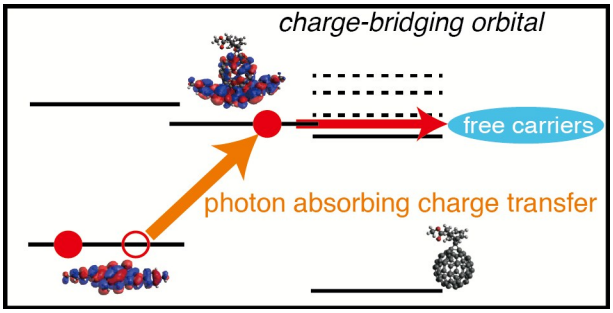

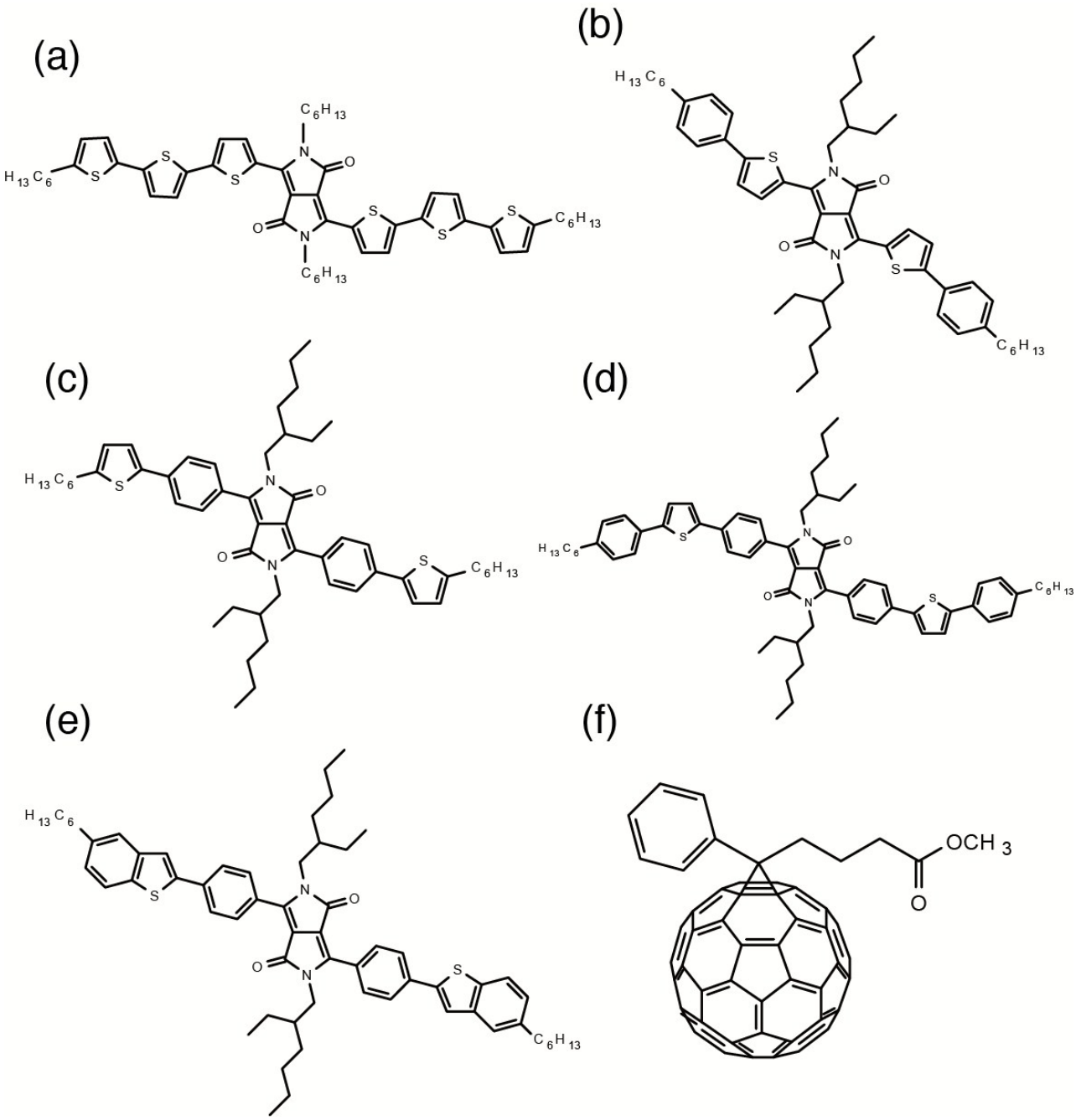

Figure 1: Chemical structures of donor (diketopyrrolopyrrole derivatives) and acceptor (PCBM) molecules studied herein. (a) D1, (b) D2, (c) D3, (d), D4, (e) D5, and (f) PCBM.

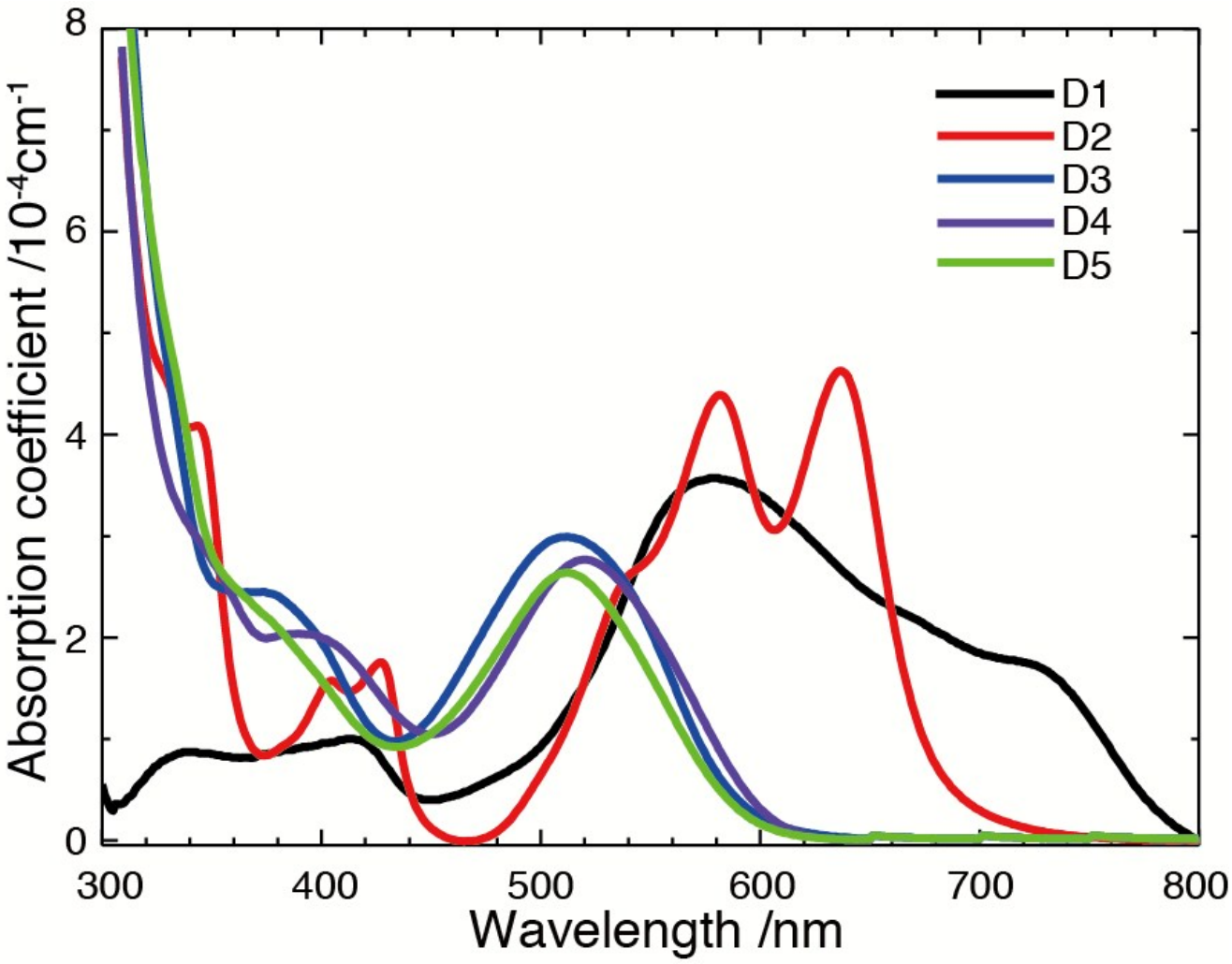

Figure 2: Experimental UV-Vis absorption spectra for diketopyrrolopyrrole derivatives recorded as solid thin films.

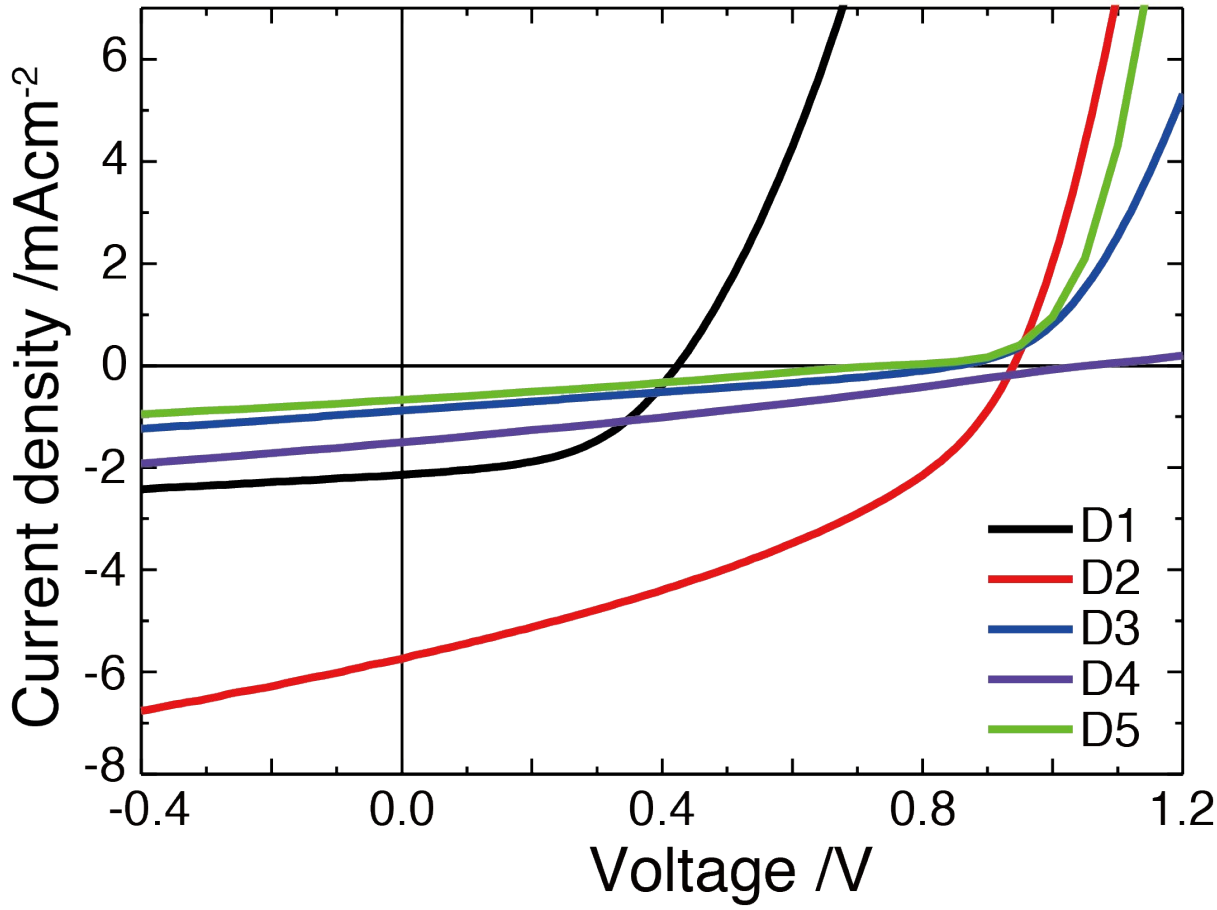

Figure 3: Experimental J-V characteristics under one sun illumination for organic solar cells based on diketopyrrolopyrrole derivatives (D1–D5) and PCBM (1:1, w/w) blends.

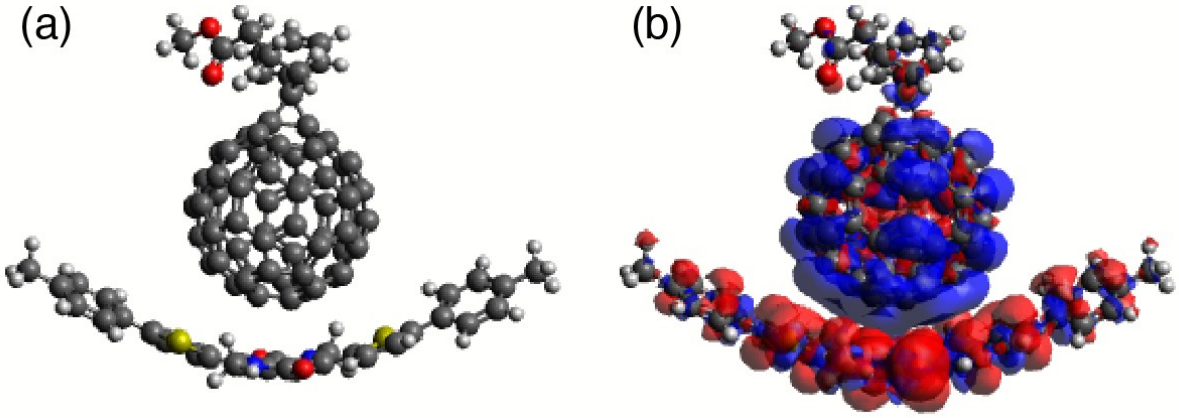

Figure 4: (a) Optimized structure on the electronic ground state of D2/PCBM. (b) Charge-transfer state of D2/PCBM, calculated by constrained HF. Densities of transferred electron and remaining hole in the charge-transfer state of D2/PCBM are depicted in blue and red, respectively.

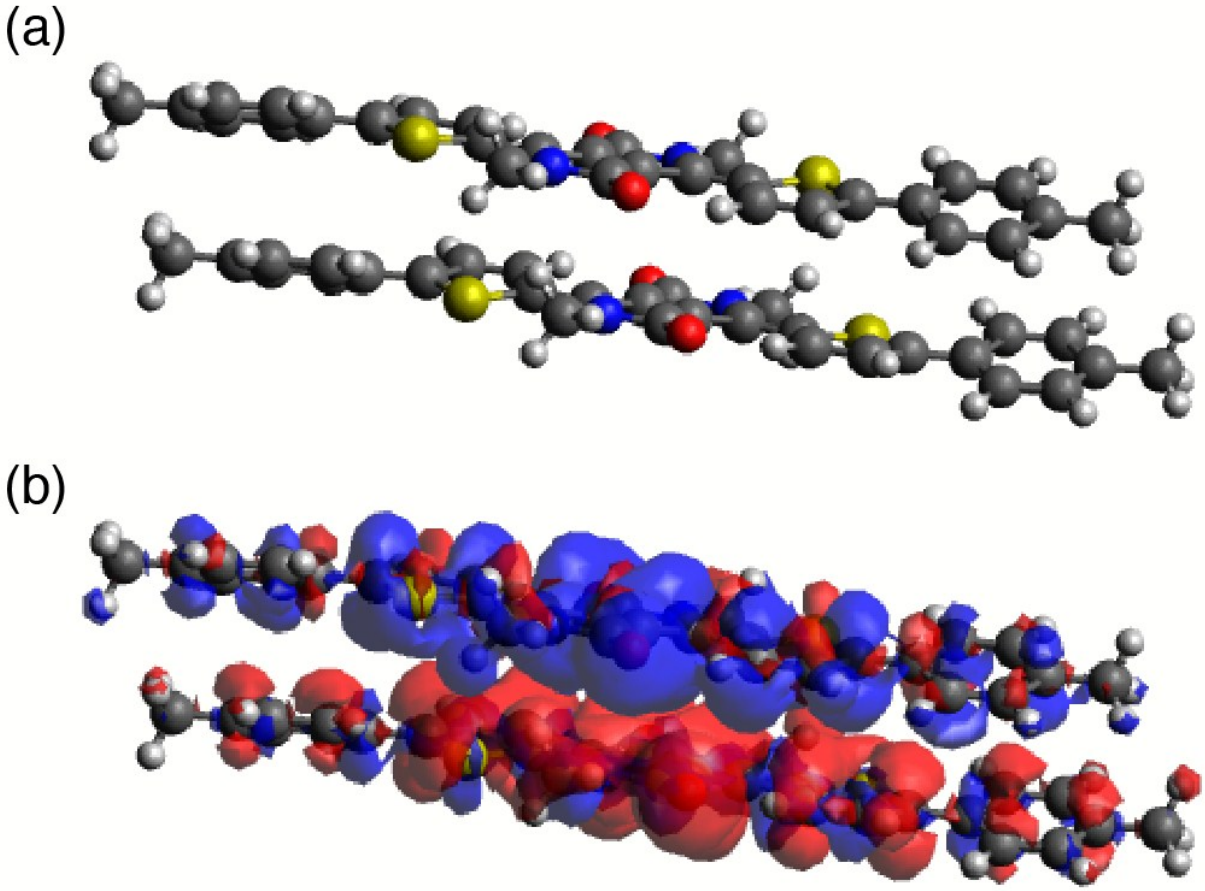

Figure 5: (a) Optimized structure on the electronic ground state of D2-dimer. (b) Hole densities before and after the hole transfer in the D2-dimer are depicted in blue and red, respectively.

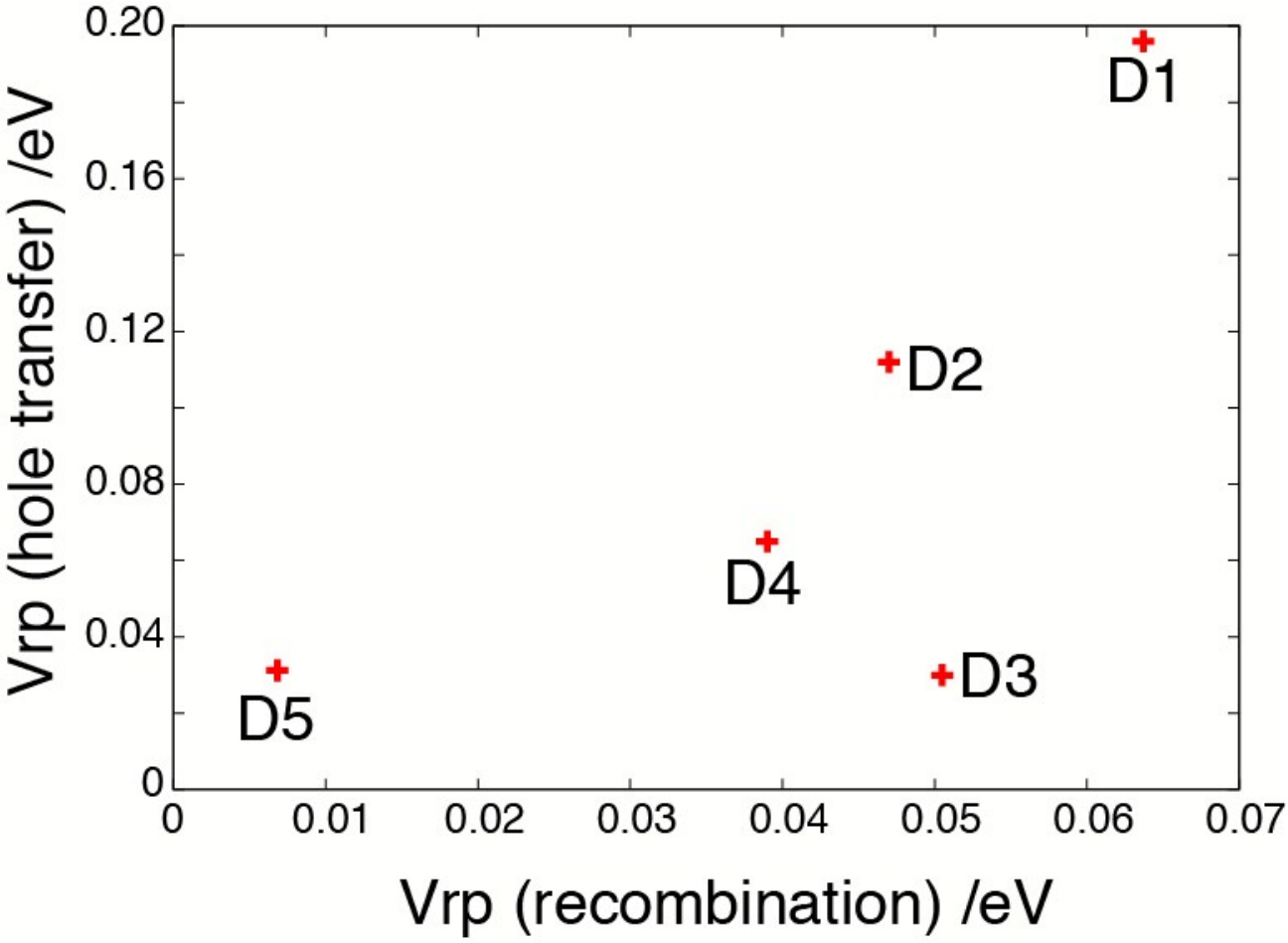

Figure 6: Electronic couplings of recombination for each DPP-derivative/PCBM complex vs hole transfer for the dimer of each DPP derivative.

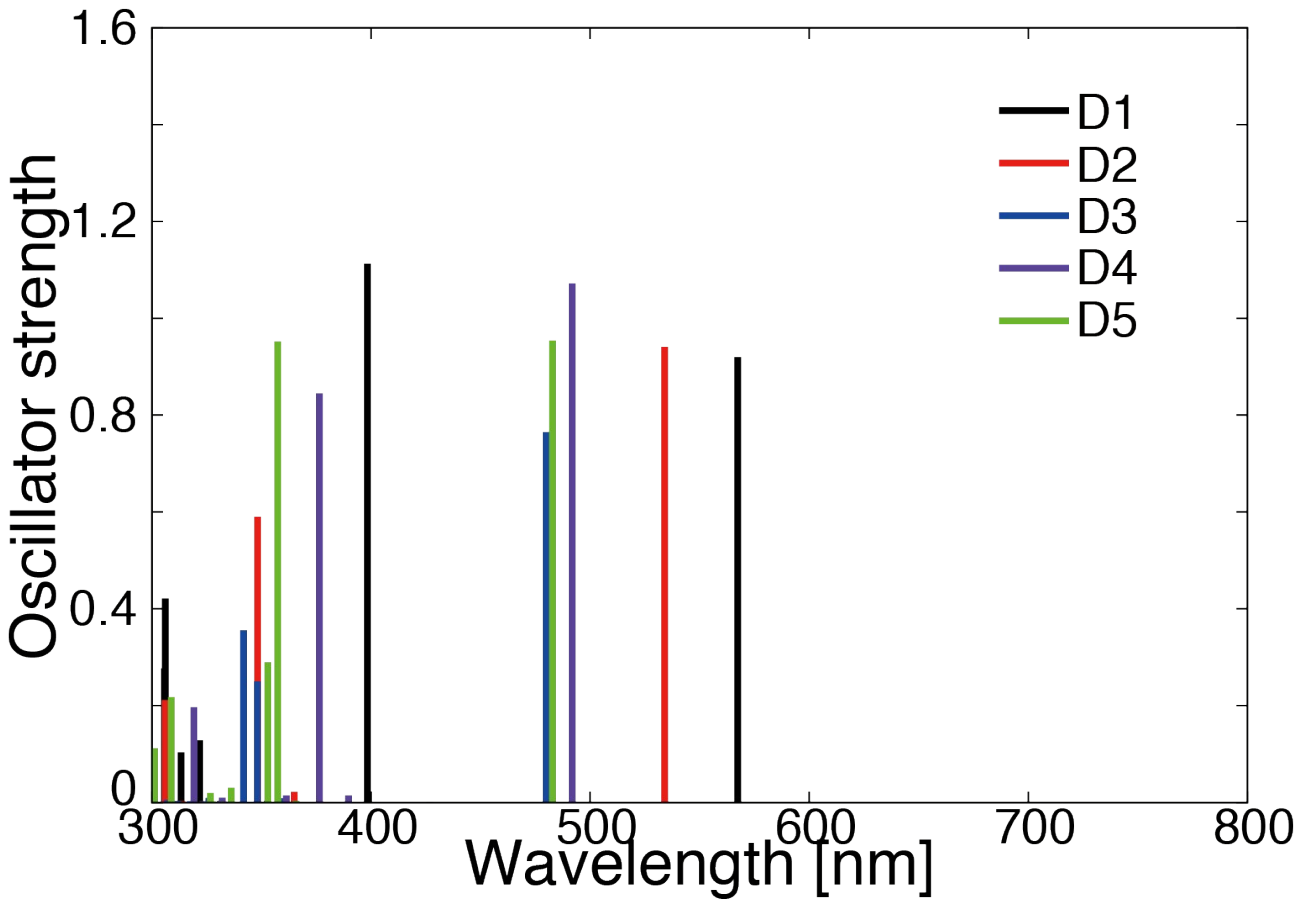

Figure 7: Calculated UV-Vis spectra for D1–D5 by PM3/CIS.

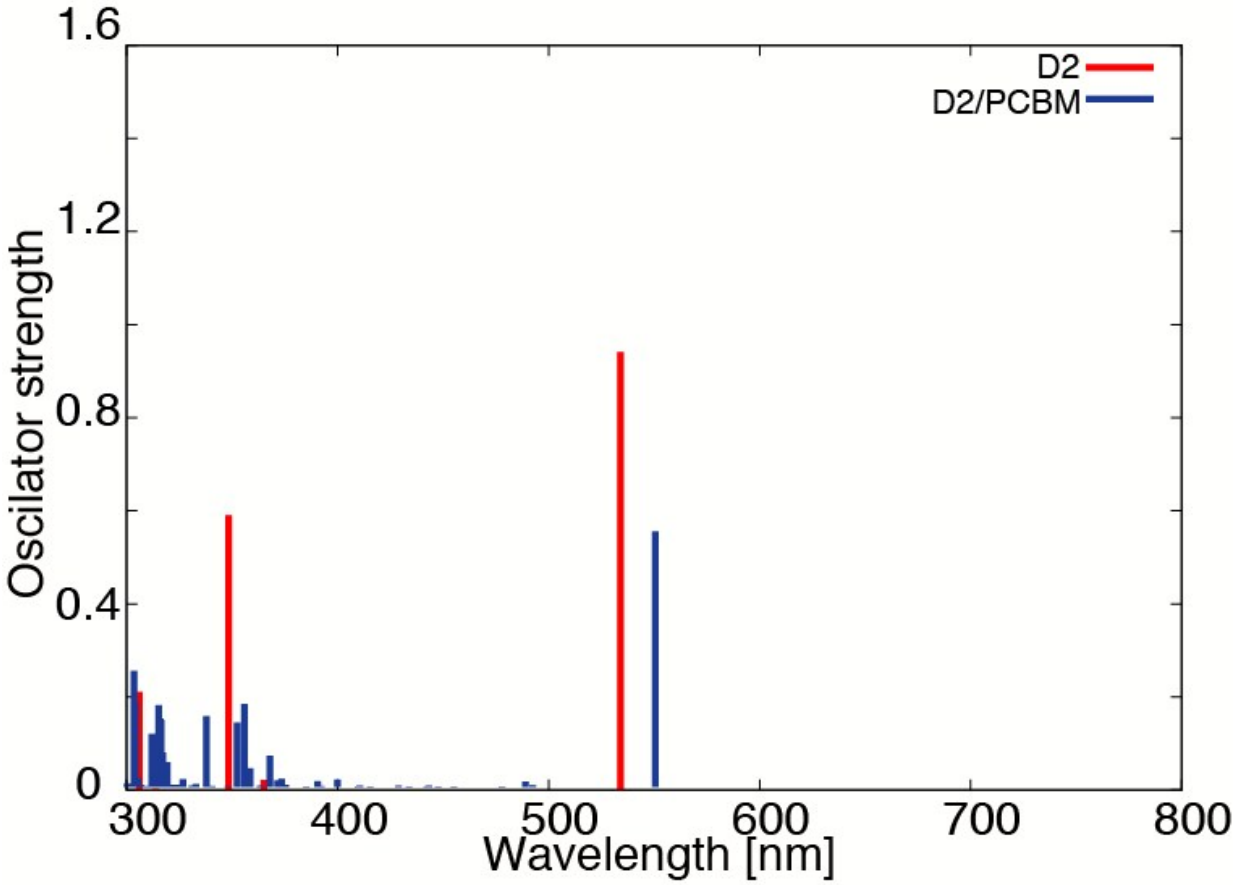

Figure 8: Calculated UV-Vis spectra by PM3/CIS for D2 (red) and D2/PCBM complex (blue).

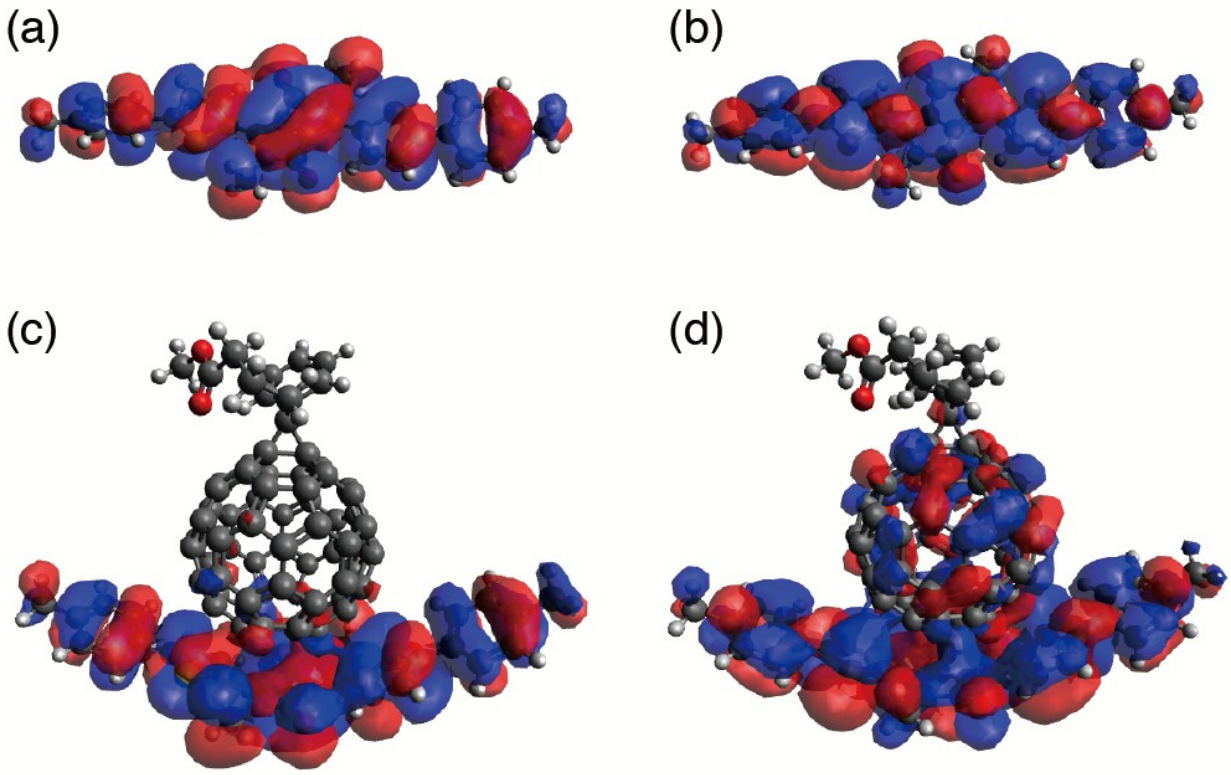

Figure 9: (a) HOMO of D2. (b) LUMO of D2. (c) HOMO of D2/PCBM complex. (d) LUMO+5 of D2/PCBM complex. These MOs are calculated by PM3.

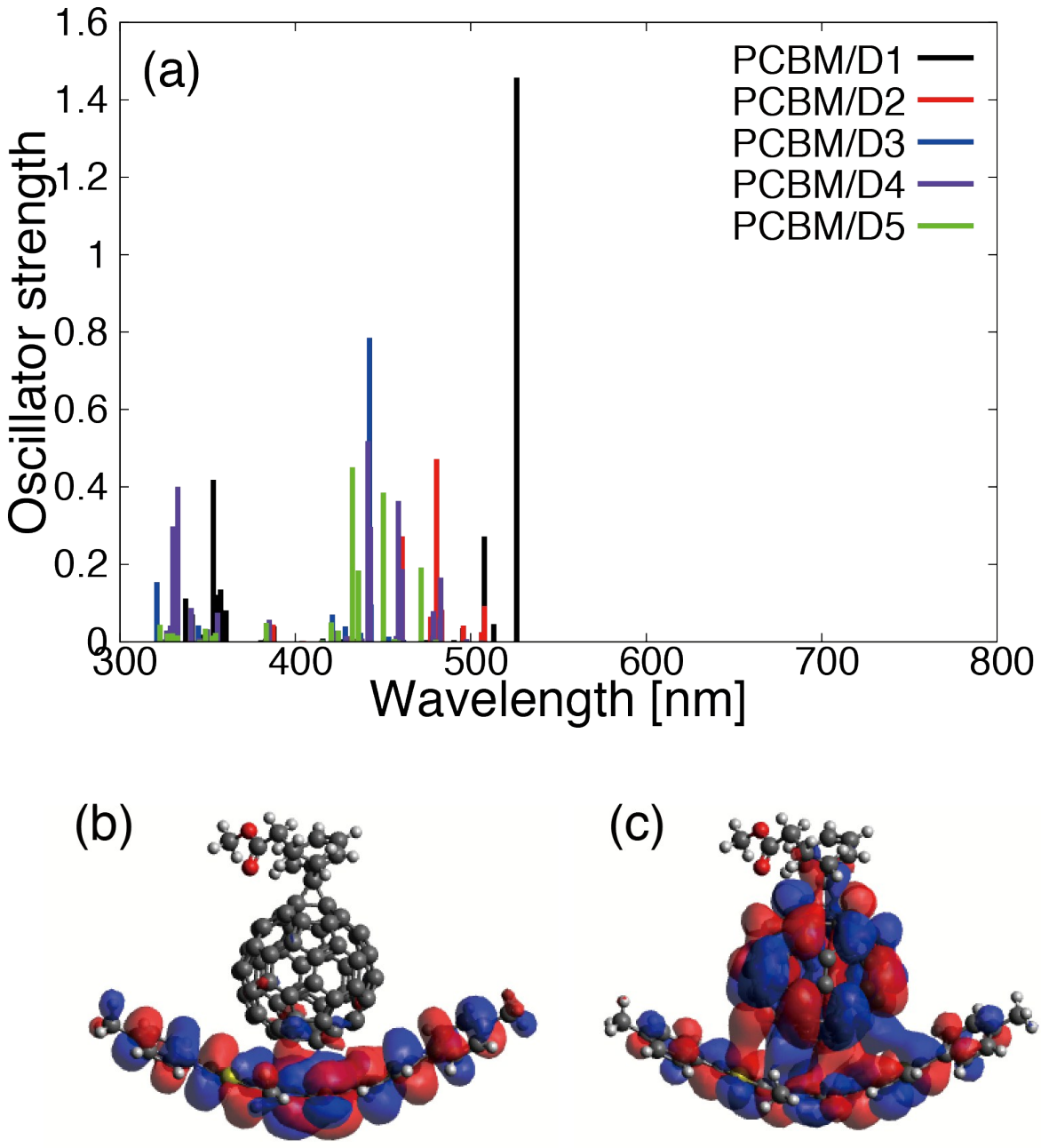

Figure 10: (a) Calculated UV-Vis spectra for PCBM/D1 – PCBM/D5 by TDDFT/CAM-B3LYP/6-31G*. (b) HOMO of PCBM/D2. (c) LUMO+2 of D2/PCBM complex.